AdVanced Aerodynamic Tools for lArge Rotors

D4.7: Turbulence Intermittency

C. M. Schwarz (ForWind)

September 26, 2016

Agreement n.: FP7-ENERGY-2013-1/n° 608396
Duration: November 2013 to November 2017
Coordinator: ECN Wind Energy, Petten, The Netherlands

supported by:

This project has received funding from the European Union's Seventh Programme for research, technological development and deomstration under grand agreement No FP7-ENERGY-2013-1/n° 608396

AdVanced Aerodynamic Tools for lArge Rotors

Document information

Document Name:	Final report D4.7: Effect of turbulence intermittency on wind turbine loads
Confidentiality Class:	XX
Document Number:	D4.7
Editor:	C. M. Schwarz (ForWind)
Contributing Authors:	**ForWind**: C. M. Schwarz, S. Ehrich **Fraunhofer IWES:** P. Thomas
Review:	S. Voutsinas (NTUA)
Date:	September 26, 2016
WP:	4
Task:	T4.2 Aeroelastic analysis of the reference wind turbine

AdVanced Aerodynamic Tools for lArge Rotors

Table of contents

1 Introduction

Deliverable D4.7 is dedicated to the effect of turbulence intermittency as part of work package WP4. This final report summarizes the findings and advancements made with respect to this subject within the scope of the AdVanced Aerodynamic Tools for lArge Rotors (AVATAR) project. The deliverable was designed to be carried out by the partner ForWind solely – during the course of the work, additional results were contributed by the partner Fraunhofer Institute for Wind Energy and Energy System Technology (IWES). In this section an introduction into the problem at hand, as well as an overview on previous related studies is given. Section 2 provides an outline of the underlying strategy chosen to address the task. Further on, results are presented and discussed in section 3. Section 4 concludes this report and summarizes the advancements and findings. Finally, section 5 points towards open questions and further work.

Turbulence intermittency

It is well-known that the statistics of wind velocity increment time series $\delta u_\tau(t)$ (c.f. Eq. 1), exhibit a non-Gaussian behaviour, see e.g. Böttcher et al. [1] or Vindel et al. [2]. This phenomenon is herein referred to as "intermittency". It must not be confused with non-Gaussian behaviour of wind velocities themselves, as one needs to distinguish carefully between the one-point statistics of wind velocities and the two-point statistics of their increments. A comprehensive introduction into the corresponding statistical framework is given by Morales et al. [3].

$$\delta u_\tau(t) = u(t+\tau) - u(t) \tag{1}$$

In order to make this phenomenon more accessible, a short procedure is outlined, which allows visualizing the deviation from a Gaussian behaviour:

1. Obtain a wind velocity time series of atmospheric turbulence (e.g. by measurement)
2. Select of an appropriate value for the time lag τ of interest
3. Generate of the increment time series $\delta u_\tau(t)$ according to Eq. 1
4. *Optional:* Often an increment time series is normalized by it's standard deviation, in order to compare the behaviour for different values of τ in a consistent way
5. Perform a statistical analysis of the resulting time series by construction of a histogram with appropriate binning
6. Plot the resulting histogram using a logarithmic scaling for the probability densities

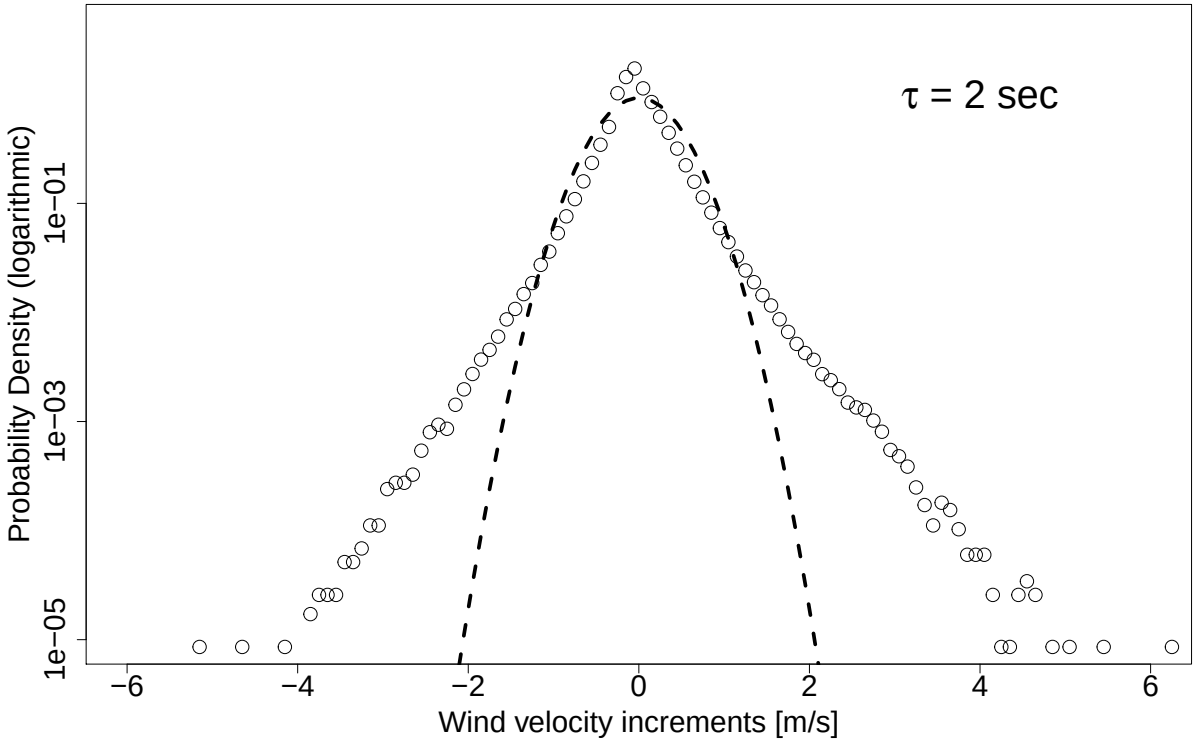

Figure 1: *Circles:* Probability densities of wind velocity increments $\delta u_{\tau=2}$ (not normalized) obtained from measurement data at FINO 1 met mast [4] for a time lag $\tau = 2$ seconds. *Dashed line:* Normal distribution with the same standard deviation as $\delta u_{\tau=2}$ and zero mean.

7. Additionally plot the probability density function of a Gaussian process with the same mean and standard deviation as $\delta u_\tau(t)$, cf. Fig. 1

Fig. 1 exemplarily shows the probability densities (circles) of velocity increments $\delta u_{\tau=2}(t)$ for a measured wind velocity time series $u(t)$. The underlying data set was measured over a 14 day period in January 2006 at FINO 1 met mast [4] (Research platforms in the North Sea and Baltic Sea, germ. abr. FINO). A comparison with a Gaussian probability density function (dashed line) clearly shows the non-Gaussian, but heavy-tailed distribution of the increments for the measured data set, especially when recalling the fact that the scaling is logarithmic. Böttcher et al. [1] give a demonstrative numerical example: The authors find a deviation between measured data and a normal distribution in the order of 10^6 for events corresponding to 7 standard deviations (for details see Ref. [1]). This difference is presented as follows: The Gaussian statistics predict this event to occur every 500 years, while the data indicates a recurrence of about five times a day. This example motivates the presented work, as super-Gaussian increment statistics are not considered in common wind models to the author's best knowledge. By neglection of intermittency these models imply

Gaussian behaved increment statistics. From an intuitive stand point, the under prediction of extreme gust recurrences by Gaussian statistics is possibly distorting the prediction of a wind turbine's performance and loading. With respect to a wind turbine's power generation, evidence for the importance of intermittency has been reported (see e.g. [5, 6]).

With respect to loading, varying results have been found in previous works, wherefore this study will focus on wind turbine loads. Mücke et al. [7] analysed rain flow counts of torque time series, obtained from Blade-Element-Momentum (BEM) based computations with synthetic intermittent wind fields. These fields were created with a wind field generator according to Kleinhans [8]. Good agreement between these results and measurement data was found, but no clear conclusion regarding fatigue loads was drawn. Further load sensors were not considered. Gontier et al. [9] compared different wind models (including the Kleinhans model [8]) utilizing BEM simulations and focusing on blade load sensors. It was found that the intermittent fields used in the study led to differences in the loads, although the authors denied a clear trend in their results. Recently, Berg et al. [10] conducted a comparison between Gaussian and intermittent fields based on wind fields obtained from Large Eddy Simulations (LES). These were processed through a BEM based aero-elastic code. The authors did not find any significant differences between both types of fields and argue that the extreme increments of the intermittent wind fields are entirely damped out by the turbine, as they occur predominantly on small time scales. The authors come to the conclusion that intermittency is irrelevant with respect to wind turbine loads. In summary, the findings of the cited studies diverge in their conclusions. It is therefore aimed to shed light into this subject.

2 Methodology

2.1 Task description

This deliverable aims at investigating different open questions related to turbulence intermittency with respect to wind turbine loads. Firstly, it shall be investigated, whether different aeroelastic codes process intermittent fields in a comparable and consistent manner. On the one hand, this pre-examination is needed in order to draw any profound conclusions from deeper analysis of the generated data. Further it matches the general scope of task T4.2 within the AVATAR project, as T4.2 is regarded as a "comparison platform" for different aero-elastic codes. Hence, it is aimed to contribute as well as gain from the code comparisons within T4.2. Secondly, a fundamental investigation on the progression of the statistics of interest within the wind turbine model and aero-elastic code is conducted. This investigation aims at answering, how non-Gaussian increment statistics are processed between different wind turbine components, as numerous dynamics affect the highly sensitive increment statistics and distort seemingly simple relations. Lastly, an assessment of the resulting loads in terms of common, practical load quantities such as Damage Equivalent Loads (DEL) shall be carried out in order to judge the overall importance of intermittency with respect to loads. In summary, the key questions in this study are the following:

1. Do different aeroelastic codes deliver comparable results with respect to intermittency?
2. How are the dynamics processed through out the system embodied by the wind turbine model and the aero-elastic code?
3. What impact does the consideration of intermittency have in terms of DEL?

2.2 Test case

As a test case for the outlined study the AVATAR Reference Wind Turbine (RWT) in below rated conditions at 9 $\frac{m}{s}$ (generator region 2) was chosen. This selection is motivated in order to avoid further complications of wind turbine dynamics within the pitch controlled wind speed regime on the one side and discontinuous behaviour near cut-in wind speed on the other. It is emphasized that the conclusions of this report may change notably when considering other wind speeds. Hence conclusions drawn within this study cannot be extended trivially to other operational regimes of the RWT. Details regarding the utilized wind fields are discussed in the following section; an overview is given in table 1.

2.3 Generation of wind fields

For the generation of intermittent wind fields a generator according to Kleinhans [8] is used. It bases on the application of Continuous Time Random Walks (CTRW) by projecting a time scale s, intrinsic to the model, onto the physical time scale t utilizing a Lévy process. The

Mean wind velocity (main component)	$9\frac{m}{s}$
Mean wind velocity (vertical component)	$0\frac{m}{s}$
Mean wind velocity (lateral component)	$0\frac{m}{s}$
Turbulence intensity (each component)	10 %
Wind shear	none
Type of energy spectrum	CTRW
Sampling frequency	20 Hz
Time span	1 h $\hat{=}$ 3600 sec
Data points in time	72.000
Vertical grid size	5 m
Horizontal grid size	5 m
Grid points	45 x 45
Reference length scale	42 m

Table 1: Overview over the generated wind fields

velocity fields are initially constructed for the intrinsic time scale s and exhibit Gaussian behaviour. By the translation onto the physical time scale t, non-Gaussian increment statistics are introduced into the data. This model has successfully been applied in previous studies [7, 9]. In contrast to common wind models, it is not based on a spectral representation of the wind, therefore a comparison against this type of models is delicate. So intermittent CTRW fields are compared to Gaussian CTRW fields, aiming at isolating the effect of intermittency in a reliable fashion. Recently, modifications to the model as used previously [7, 9] were brought forward. These include a modification of the spectral properties, the spatial correlations and an elimination of three model parameters by constraints made to the power spectral densities of the generated time series by Ehrich (publication to follow).

In order to resolve the statistical features of interest, a relatively high amount of data is required. The underlying wind fields of this study cover a time span of one hour featuring a sampling frequency of 20 Hz, resulting in 72.000 data points in time. The spatial domain is discretized equidistantly using a 45x45 grid featuring a mesh size of dx = dy = 5 meter, covering a 220 meter (corresponding to 105% of the rotor diameter) by 220 meter area. Further on, the fields feature a turbulence intensity of 10% and a reference length scale of 42 meter in accordance with International Electrotechnical Commission (IEC) standard for wind turbines 61400-1 [11]. The generated time series feature an own characteristic spectral behaviour, which differs from commonly accepted wind representations according to Mann [12] or Kaimal et al. [13]. It was assured that all fields used within this study feature the same spectral properties. This is achieved by a modification of the field's spectra in Fourier space. We point out that the fields may not feature power spectra in accordance to the IEC standard, but still allow for a consistent isolation of the effect of intermittency, since spectral properties are comparable. The fields can be considered as isotropic and do not feature a

wind shear for the sake of simplicity. A wind shear would introduce a sinusoidal dynamic into the wind turbine system and must be considered in further studies, considering practical applications.

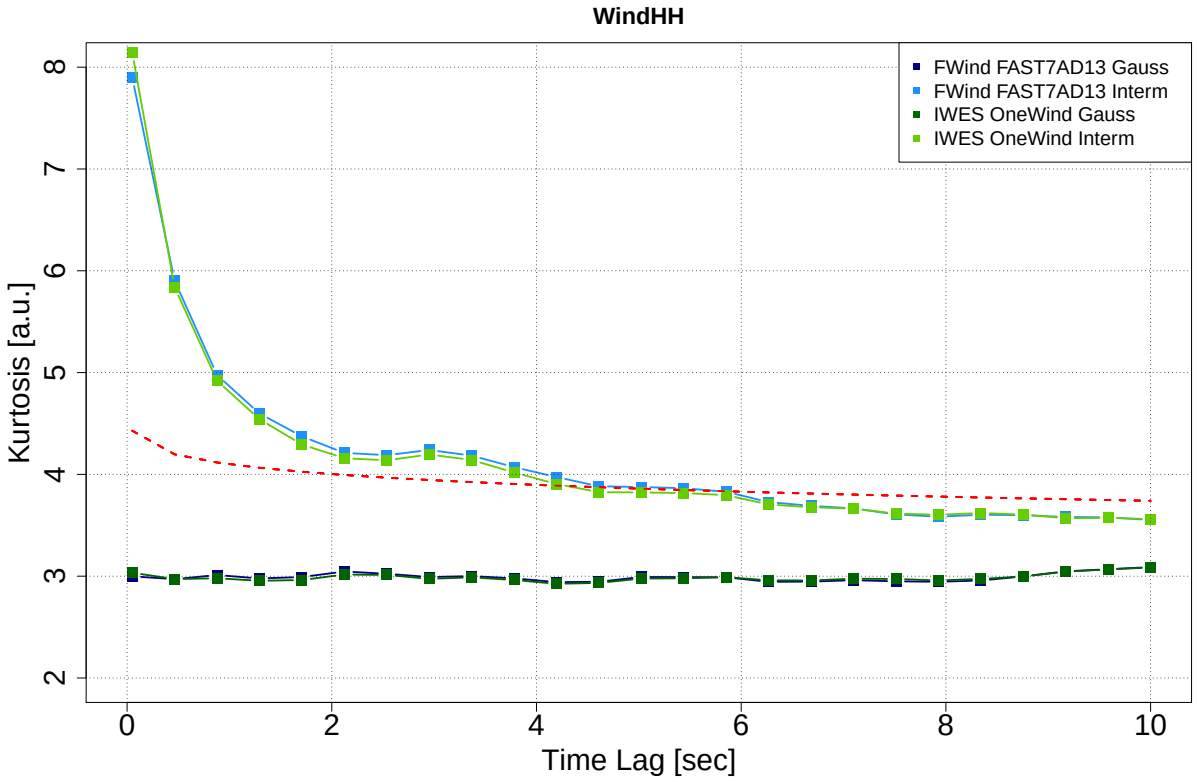

Figure 2: Kurtosis of the probability density of increment time series for sensor `WindHH` for all codes and types of fields. *Red dashed line:* Theoretical relation between the kurtosis F and time lag τ as given by Eq. 4.

The "strength" of intermittency is captured by the kurtosis of the increment probability densities over a range of time lags τ as shown in Fig. 2. A more comprehensive explanation how to obtain these values is given by Morales et al. [3] and recapped briefly in section 3.2. Fig. 2 representatively shows the kurtosis for the sensor `WindHH` (wind speed at hub height) for both wind fields after being processed by the codes involved in this study. Within the used modelling approach it is not possible to prescribe the kurtosis a priori. A comprehensive parameter study resulted in the present parameter set and aims at modelling atmospheric turbulence as close as possible. As outlined by Morales et al. [3], the so-called λ^2 and the time lag τ are related as follows:

$$9\lambda^2 \propto \mu \ln(\tau) \tag{2}$$

Herein, λ^2 is directly related to the kurtosis F (cf. Eq. 5) of the increment time series:

$$\lambda^2 = \frac{\ln(F(\delta u_\tau/3))}{4} \tag{3}$$

Further, the value of μ in Eq. 2 is empirically found as $\mu \simeq 0.29$ [3]. From equations 2 and 3 a relation between F and τ can easily be formulated

$$F \propto \tau^{\frac{4}{9}\mu}. \tag{4}$$

Fig. 2 clearly shows the imperfect match between the synthetic intermittent fields and the relation given by Eq. 4 on small time scales $\tau < 2$ sec. As mentioned before, a careful analysis of the modelling parameters resulted in the set-up as used in this study. To the author's best knowledge, there is no approach to model intermittent wind fields with a prescribed kurtosis $F(\tau)$, wherefore improvements were not possible within the time frame of this project and the methodology is considered state of the art. In the range 2 sec $\leq \tau \leq$ 10 sec, the data seems to agree reasonably with the theoretical model. Larger time scales than $tau = 10$ sec are not considered in this work, as intermittency is mostly related to small values of τ. The selected range of time lags τ is considered to be sufficient as it covers the average period of the rotor revolution $\tau_{1\mathrm{P}} \simeq 7.9$ sec and the time scale corresponding to the reference length scale of the turbulent field $\tau_{\mathrm{refL}} \simeq 4.67$ sec (applying Taylor's Hypothesis of "frozen" turbulence).

2.4 Description of codes

Partner	**ForWind**	**Fraunhofer IWES**
Code	FAST 7 & AeroDyn 13	OneWind Modelica Library
Modelling of blade structure	mode shape representation, limited to 6^{th} degree polynomial, no torsional DoF	mode shape representation, unlimited
Modelling of tower structure	see above	see above
Induction	standard (no GDW), swirl induction	standard (no GDW), swirl induction
Turbulent wake state correction	Glauert	as in Bladed v4 [14]
Skewed inflow correction	based on Glauert, Pitts & Peters	based on Glauert, Pitts & Peters
Tip/Root loss	Prandtl	Prandtl
Dynamic stall	Beddoes & Leishman	Øye

Table 2: Summarizing overview over the code set-ups used in D4.7

The deliverable was initially planned to be carried out by the partner ForWind solely. It became evident during the course of the investigations that comparisons of different code

performances with respect to intermittency are desirable, in order to have reference results to draw conclusion from. Within the limited time frame, only the partner Fraunhofer IWES was able to contribute to this study. In the following, the aero-elastic codes used are presented. A quick overview is given in table 2.

2.4.1 Forwind: FAST 7 & AeroDyn 13

Results provided by partner ForWind were produced with the open-source code FAST (v7.02.00) [15] in combination with Aerodyn (v13.00.02) [16]. The code was used in a baseline configuration, besides a recalibrated Beddoes-Leishman dynamic stall model according to Pereira et al. [17]. The used code is certified and well-known within the wind energy community. Details can be found in the corresponding sources. Noteworthy is the limited structural modelling. Torsional deformation of the rotor blade and the tower are not modelled. Further on, the *NewTower* function, which is based on a potential flow computation was utilized to model the tower blockage effect.

2.4.2 Fraunhofer IWES: OneWind

Abstract
The OneWind®Modelica Library includes all major components needed for load calculations of current onshore and offshore wind turbines and is freely available for academic use. Models for environmental conditions and their respective influences on the structure are included (Table 1). The library constitutes a large effort in creation of a highly coupled multiphysics model with the modelling language Modelica. The source code of the library is available and can be adopted to application-specific components. This makes it possible to exchange / modify existing functionalities and to further expand the code by user-specific functionalities. The aim of this library is to use it for certification load case calculation by IEC 61400-1 and 61400-3 and GL Guideline for the Certification of Wind Turbines. Results obtained with this library are continuously compared to results from the several projects in the IEA Offshore Code Comparison Collaboration [18] and continually verified with FAST [15] and Bladed [19].

Wind turbine system simulation
The OneWind Modelica Library is able to perform aero-hydro-servo-elastic simulations of wind turbine systems, i.e. it comprises wind-inflow, aerodynamics (aero), waves and currents, hydrodynamics (hydro), control system (servo) and structural dynamic (elastic) models in a time domain coupled simulation environment. The models are grouped according to wind turbine components as seen in Fig. 3 for an offshore wind turbine. This figure shows the model instances and corresponding interactions for the main wind turbine components: the rotor (with subcomponents of blade and hub), the tower, the substructure, the nacelle (with the subcomponents of drive train and generator), operating control, wind, waves, ice and soil. To simulate at different levels of detail, several models for almost every wind turbine

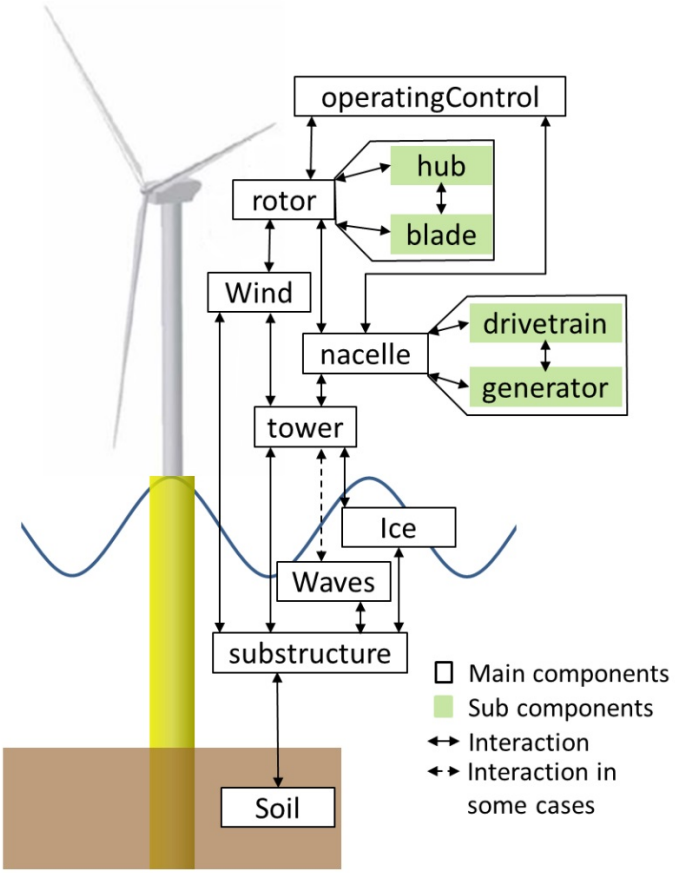

Figure 3: Major components of an offshore wind turbine in the OneWind®Modelica Library

component are available.

Components of the Library

The particular components can be implemented independently due to the multibody system based structure of the OneWind Modelica Library. In Table 6 (see Appendix) a brief overview of the components of the OneWind Modelica Library is given. Further information on the models can be found in [20] and [21].

Wind models

Deterministic and stochastic wind models are available. Deterministic wind uses several gust models. The stochastic wind data is read from the binary or ASCII file produced by

TurbSim [22] format.

Aerodynamic models

The aerodynamic load calculation uses either the blade element momentum (BEM) theory or the general dynamic wake method (GDW). The BEM theory is implemented as an iterative algorithm while the GDW is a set of differential equations. For the BEM, corrections for the dynamic wake and the dynamic stall can be used. Dynamic stall correction is also available for GDW.

Control system

The operating control system is implemented based on [23] and consists of a PI-pitch algorithm to control the power production above rated rotor rotation speed and a generator-torque controller which requests the counter torque from the electrical generator due to rotor torque. Several speed filters are available.

3 Results

At first, the first and second statistical moments of a selected list of sensors are compared. In doing so, insight regarding the comparability of the data sets at hand is obtained. In the following, two-point analyses in the context of intermittency are conducted in order to describe and judge the impact of this statistical feature, as well the codes' abilities to process the wind fields in a consistent manner. Finally, a fatigue load analysis is conducted. As outlined above, within this deliverable the focus is upon wind turbine loads. The intermittent dynamics are expected to be felt predominantly by sensors with high sensitivity to the axial wind speed component. Hence, dynamics of wind velocities and loads corresponding to the vertical or lateral directions are not considered in this study. Additionally, key performance sensors such as the rotor torque are monitored. A small set of sensors was selected for this study:

- `WindHH`: Hub height wind speed (main component) $[\frac{m}{s}]$
- `RotThrust`: Rotor thrust [kN]
- `RotTorq`: Rotor torque [kNm]
- `GenPow`: Generator power [kW]
- `TwBaseFA`: Tower base bending moment (fore-aft) [kNm]
- `RootOOP`: Blade root bending moment (out of plane) [kNm]
- `RootIP`: Blade root bending moment (in plane) [kNm]

3.1 One-point statistics

Fig. 4 shows the mean values obtained from time series of each of the listed sensors for all codes and wind fields. For better visualization, all mean values are normalized by the mean value obtained from the Gaussian data set provided by the partner ForWind. It is emphasized that the values taken for normalization do not stand out in any way against results and were arbitrarily selected as a reference.

A high agreement (around 0.1% difference) between the mean hub height wind speeds (main component) for both the Gaussian and intermittent wind fields is displayed. The wind fields are designed to have exactly the same average wind speeds. Marginal differences are likely to arise from the internal calculation of the `WindHH` within the corresponding codes. These might differ in the number of grid points to be taken into account or possibly even in the location of the reference point in the rotor plane. The remaining sensors show a similar trend between the Gaussian and intermittent cases.

Differences across all sensors up to approx. 15% (for `RotTorq`) between the codes can be identified. Although the codes share several common features in their modelling approaches

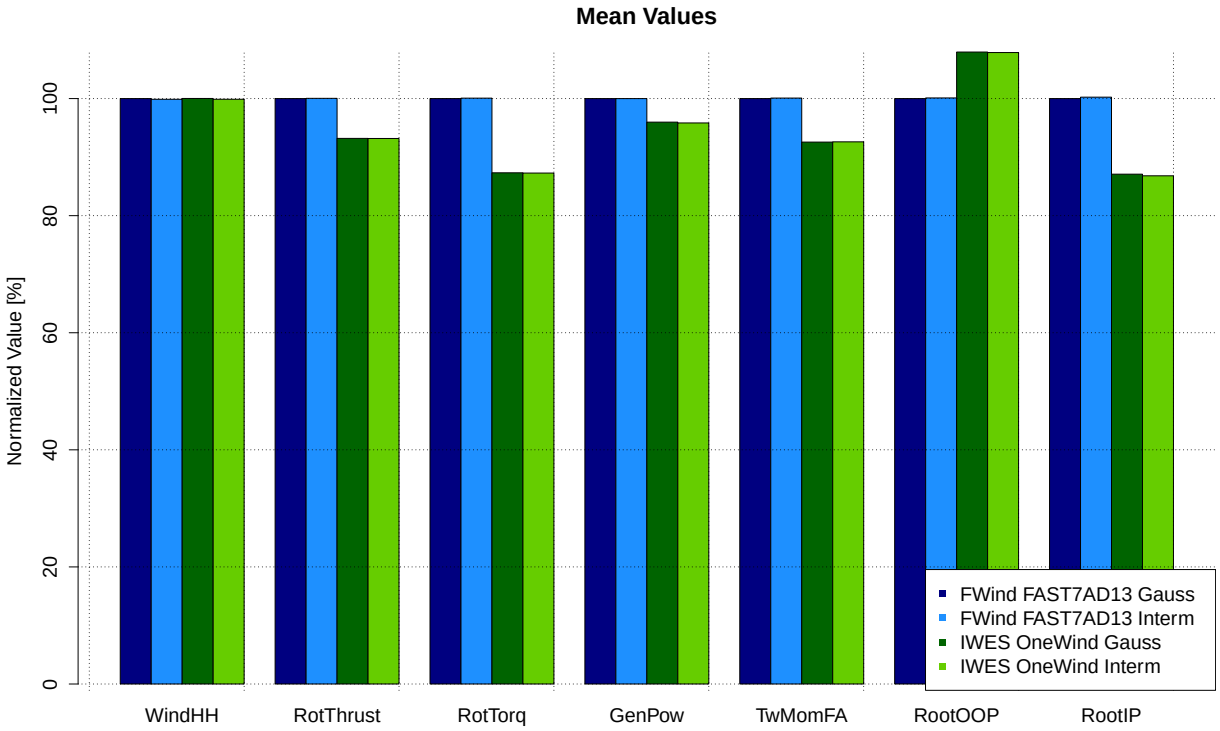

Figure 4: Comparison of mean values for all codes and fields

	ForWind Gaussian	ForWind Interm.	IWES Gaussian	IWES Interm.
`WindHH`	100	99.88	100.02	99.88
`RotThrust`	100	100.04	93.20	93.18
`RotTorq`	100	100.08	87.32	87.28
`GenPow`	100	100.00	95.98	95.84
`TwMomFA`	100	100.09	92.57	92.61
`RootOOP`	100	100.11	107.95	107.86
`RootIP`	100	100.24	87.09	86.81

Table 3: Comparison of mean values for all codes and fields

there are differences in dynamic stall modelling, the torsional degree of freedom is missing in the FAST code or the number and resolution of the underlying mode shapes within structural modelling approach. Furthermore one cannot exclude the possibility of inconsistencies within the structural modelling. In particular the higher `RootOOP` mean values given by partner Fraunhofer IWES seem to not comply with the smaller `RotThurst` mean value obtained. Given the limited time frame of this deliverable, this issue could not be investigated in

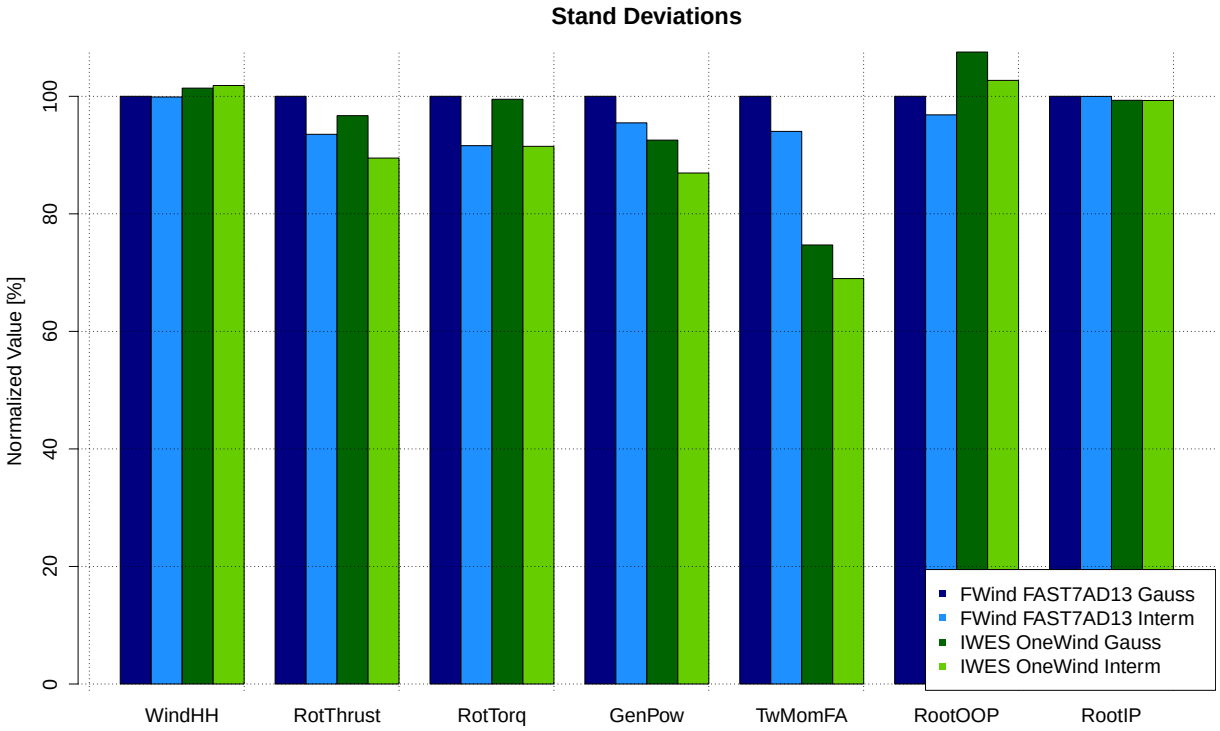

Figure 5: Comparison of standard deviations for all codes and fields

	ForWind Gaussian	ForWind Interm.	IWES Gaussian	IWES Interm.
`WindHH`	100	99.89	101.40	101.84
`RotThrust`	100	93.53	96.70	89.49
`RotTorq`	100	91.60	99.50	91.49
`GenPow`	100	95.48	92.55	86.95
`TwMomFA`	100	94.03	74.70	68.99
`RootOOP`	100	96.85	107.53	102.71
`RootIP`	100	99.98	99.32	99.23

Table 4: Comparison of standard deviations for all codes and fields

greater detail.

Fig. 5 shows an analogous comparison of the standard deviations obtained from the very same time series. Focusing on `WindHH` at first, differences between the different codes become more evident. The differences between the intermittent and Gaussian cases of partner Fraunhofer IWES are within 0.5% of each other, whereas the difference between both results of partner ForWind is around 0.1%. The quantitative difference can be judged as marginal,

but support the assumption of disparities in the calculation of `WindHH` by the respective codes, as the underlying wind fields are identical.

The overall picture given in Tab. 4 and Fig. 5 is mostly consistent with the trends of the mean values displayed Fig. 4. Notable differences emerge for `RotTorq` and `RootIP`. The mean values of both quantities (cf. Tab. 3) from the two codes differ notably, while their standard deviations seems to match well. Focusing on `RotTorq`, the codes predict different operational points, since their mean values differ from each other. Modelling differences are likely to be the reason for the different operation points. The fluctuations of `RotTorq` as reflected on the standard deviations in Fig. 5 are obviously dependent on the rotor's operation point, but should be driven by the fluctuations in the wind field fluctuations, which for both codes are statically equivalent. This gives a possible explanation for the difference in the mean and the agreement in the standard deviation for `RotTorq`.

A similar observation can be made for `RootIP`. This quantity will oscillate in a sinusoidal manner featuring a 1P frequency, due to gravity forces. This motion is superposed by smaller fluctuations arising due to wind dynamics. Hence, in all following discussions, `RootIP` needs to be considered in a different manner, as it's dynamics are dominated by a periodic, deterministic effect and only exhibits weak stochastic behaviour. This gives an explanation for the good agreement between the standard deviation of both codes. The difference in the mean value is likely to arise from differences in the structural models.

Maybe the most important observation from the comparison of standard deviations shown in Fig. 5, is the reduction of standard deviations in the intermittent cases (aside from `RootIP` due to the circumstances discussed above). A possible explanation for this effect can be found in the nature of the intermittent fields: By definition, intermittent fields will feature extreme changes in wind velocity. Sometimes these changes may occur from one moderate wind velocity level to another, as for instance an extreme jump from a moderately low wind velocity to a moderately high wind velocity in short time. Sometimes though, it will lead to extreme values of wind velocities, for instance when jumping from an average or moderately high wind velocity value to an even higher one. The extreme values obtained in the latter type of jump, constitute what is usually described as a "peak". Hence, extreme peaks will occur more often in intermittent fields than in comparable Gaussian fields and will contribute significantly to the standard deviation, as the absolute difference to the mean value enters the calculation of the standard deviation quadratically.

During the course of an aero-elastic simulation, extreme changes will not be processed into other load sensors, such as `RotThrust`, par for par: These extreme changes will be damped due to physical sources of damping (e.g. inertia) and further due to numerical sources, such as relaxation and filtering. Obviously, physical damping needs to be considered in the modelling approach. Relaxation and filtering are theoretically avoidable, but practically will occur in order to assure stable computations. Conclusively, the damping of peaks would explain why some extreme terms in the calculation of the standard deviation could be missing for the load sensors, resulting in lower values. Berg et al. [10] discuss the damping of intermittent

dynamics, as well. They conclude that the non-Gaussian dynamics are filtered away by the turbine, since they appear on length scales smaller than the rotor. As becomes evident in the discussion of two-point statistics in Section 3.2, intermittent behaviour can still be observed for different load sensors despite the presence of damping. Further research work should aim at resolving this contradiction.

3.2 Two-point statistics

In this section the two point statistics of the monitored sensors are evaluated. The main focus lies on the kurtosis (sometimes *flatness*) of probability densities of increment time series. In Section 1, the outline for a procedure was described from which one obtains the probability densities functions of increment time series for the case of wind velocity time series. Regarding load time series, the very same analysis can be conducted. In order to evaluate two-point statistics efficiently, it is convenient to reduce each of the increment probability densities to one value, the kurtosis (cf. Eq. 5), and plot it against the time lag τ.

$$F(X) = \frac{E[(X-\mu])^4}{(E[(X-\mu)^2])^2} \tag{5}$$

For an ideal Gaussian process X_{Gauss} the kurtosis has a value of $F(X_{\text{Gauss}}) = 3$. Correspondingly, processes with a kurtosis higher than three can be classified as super-Gaussian. The histograms of those processes – compared to a Gaussian process – will feature a more pronounced peak around the mean value, as well as heavier tails. Conclusively, a super-Gaussian process features more values very close to the mean and more extreme values (tails), as well. Bins corresponding to moderate deviations from the mean value are less pronounced in a super-Gaussian process. These features are vice versa for sub-Gaussian processes which feature a kurtosis less than three. In the following, the kurtosis F of increment time series $\delta x_\tau(t)$ (cf. Eq. 1) of the selected load sensors are presented in a way analogous to Fig. 2.

RotThrust

Fig. 6 shows the kurtosis $F(\tau)$ for the sensor `RotThrust`. Obviously, F (cf. Eq. 5) is highly sensitive against any kind of variation in the underlying data. Considering Table 2, fundamental modelling differences become evident, wherefore differences in the two-point statistics are generally expected. The overall picture given in Fig. 6 shows a reasonable agreement between both codes. The intermittent fields result in intermittent `RotThrust` time series.

Intuitively, a well pronounced correlation between `WindHH` and `RotThrust` may be expected, since the wind speed is the driver of the rotor thrust. Still, differences between the super-Gaussian kurtosis of `WindHH` and `RotThrust` are evident. An explanation is given by the fact that the rotor thrust is obtained from the sum of all rotor blades. Each radial section

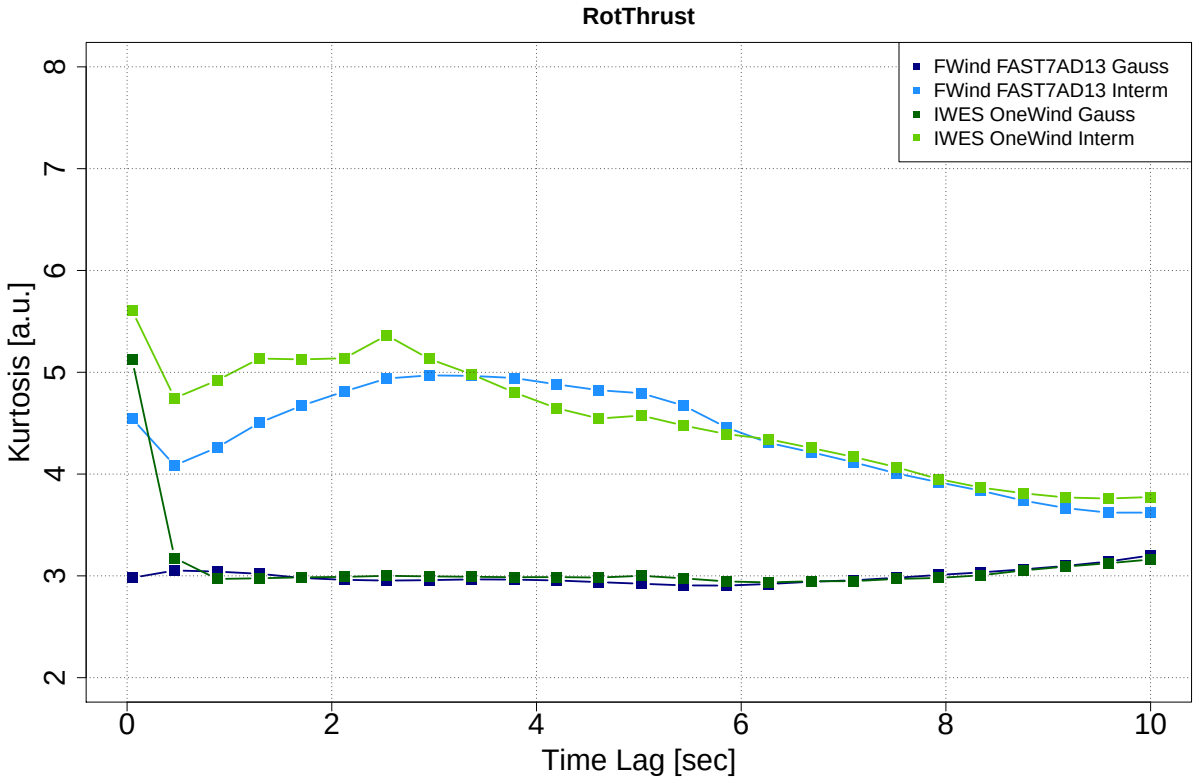

Figure 6: Kurtosis of the probability density of increment time series for sensor `RotThrust` for all codes and types of fields.

features a non-linear relation between the wind speed and the normal force, as the normal force coefficient is a non-linear function of the angle of attack. Dynamic stall modelling or other common correction models, say for root and tip-losses, will also contribute to normal force, wherefore even more differences between wind and thrust arise. Finally, the blades will experience periodic events during a rotor revolution. A phase-shifted summation of these periodic events is another reason, why the two-point statistics of `WindHH` and `RotThrust` are different. An analytic approach towards the rotor thrust supports the ideas outlined above: The rotor thrust T is given by the summation over all blades B and all radial section i of the normal forces $F_{\mathrm{normal}\,B,i}$, which are calculated as the product of the dynamic pressure $\frac{1}{2}\rho u_{B,i}^2$, the corresponding cross-section area A_i and thrust coefficient $C_{T\,B,i}$.

$$T = \sum_B \sum_i F_{\mathrm{normal}\,B,i} = \sum_B \sum_i \frac{1}{2}\rho u_{B,i}^2 A_i C_{T\,B,i} \tag{6}$$

Removing all constants from Eq. 6 allows to narrow down the dynamic components in order to gain a better understanding, how stochastic processes are transported into the wind

turbine component

$$T \propto \sum_B \sum_i C_{Ti}(\alpha_{B,i}) \cdot \left(\sqrt{\left(u_{\mathrm{rot},i}\right)^2 + \left(u_{\mathrm{wind},B,i}\right)^2} \right)^2 . \tag{7}$$

Eq. 7 can now be further modified in order to make the basic transfer process between the wind dynamics and the rotor thrust evident:

$$T \propto \sum_B \sum_i C_{Ti} \Big(\arctan \big(\frac{u_{\mathrm{wind},B,i}}{u_{\mathrm{rot},i}} \big) \Big) \cdot \left(\left(u_{\mathrm{rot},i}\right)^2 + \left(u_{\mathrm{wind},B,i}\right)^2 \right) \tag{8}$$

Straightforwardly from Eq. 8, the relation between wind and thrust dynamics is non-linear. It needs to be pointed out that u_{rot} in this context could be regarded as a highly complex function of u_{wind}, as well. The consideration above clarifies that one needs to expect differences between the increment kurtosis of `WindHH` and `RotThrust`, as they are connected in a non-linear way. Actually, the way Eq. 8 is formulated, only scratches the surface of the problem, as effects such as dynamic stall, motion due to flexible structure, tip and root loss modelling and the blades' tower-passage are "hidden" in it, as well. Additional information on how to obtain the dynamics of `RotThrust` from the dynamics of normal forces are given in the section focusing on `RootOOP`, as an insight into the sectional forces is given (cf. Fig. 8), which assists the understanding of the dynamcis of `RotThrust`, as well.

Further on, an unexpected behaviour for the smallest value of τ for the Gaussian IWES case can be observed. It is very likely that this value arises from a numerical effect, such as a time delay filtering, which can be attractive for relaxation of numerical computations. This type of non-Gaussian dynamics are not related to any kind of wind dynamics and must be classified as a numerical effect. Within this report, it shall be referred to as "numerical intermittency". Any time numerical intermittency is observed, all increment time series for the time lags $\tau \leq \tau_{\mathrm{crit}}$ can be affected, which needs to be taken into account in the assessment of the results.

Concluding the discussion of `RotThrust`, we recall the discussion of damped fluctuations within Section 3.1. A damping of peaks was assumed to be the likely reason of the reduced standard deviations for the intermittent data. Now, considering two-point statistics, it becomes evident that differences between both types of fields are still very evident, despite the damping of the one-point statics of `RotThrust`.

RootOOP

Fig. 7 shows the kurtosis of the increment probabilities for `RootOOP`. As previously, a satisfying agreement between both codes can be observed. Further on the simulations provided by IWES display numerical intermittency on time scales $\tau \leq 1$ sec, as both the intermittent and

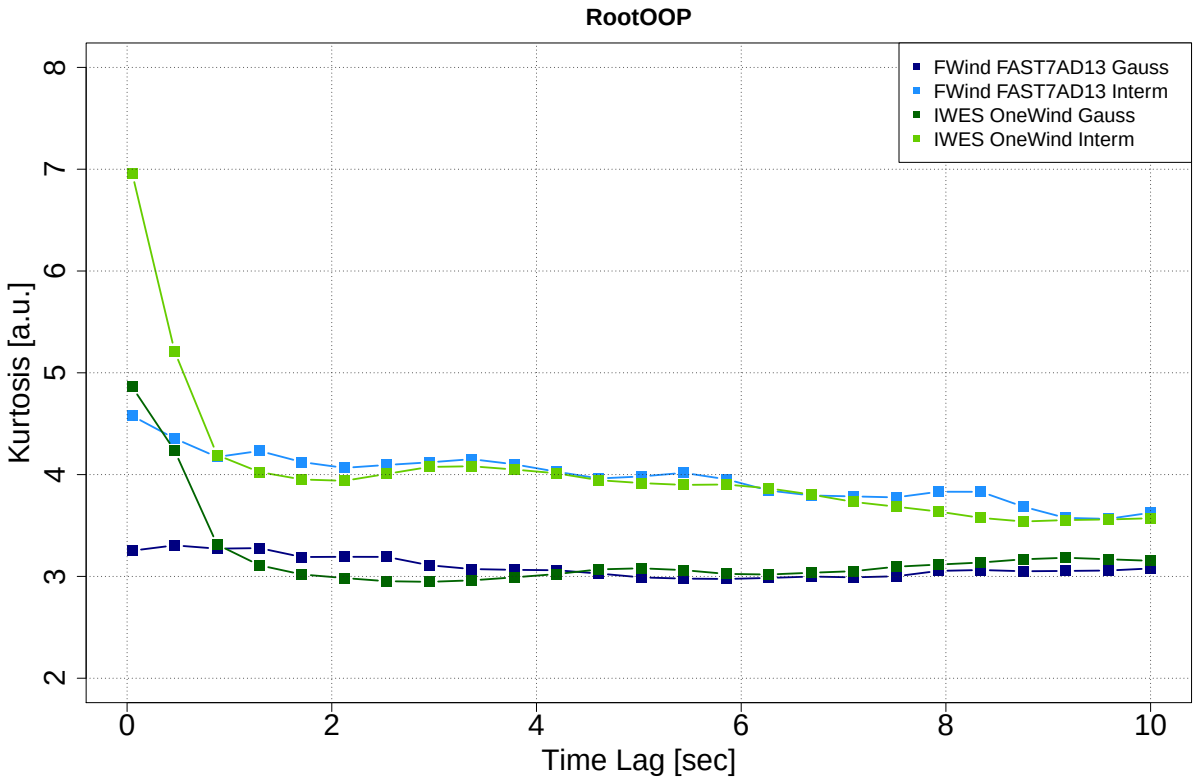

Figure 7: Kurtosis of the probability density of increment time series for sensor `RootOOP` for all codes and types of fields.

the Gaussian field show a comparable increase in kurtosis on these time scales. The overall picture is significantly different from the dynamics of `WindHH` and `RotThrust` (Figs. 2 and 6), as the kurtosis for `RootOOP` exhibits smaller values in the range of $F \simeq 4$ over a wide range of time lags τ. `RootOOP` is obviously driven by the dynamics of outboard sections, as absolute forces are greater outboards due to the radially increasing absolute inflow velocity. Additionally, the lever in this case is the radius. In Fig. 8 the kurtosis of the increment time series of normal forces for the intermittent case by partner ForWind are presented. Comparing the behaviour of `RootOOP` (Fig. 7) with the dynamics of the sectional normal forces (Fig. 8), a good agreement is found, especially for the outboard sections. Inboard sections are dominated by a relatively strong tower-passage effect, which imposes a dominant sinusoidal behaviour on the normal force time series of these sections, which results in a sub-Gaussian behaviour on scales below the 1P frequency $\tau < \tau_{1\mathrm{P}} \simeq 7.9$ sec. Time scales corresponding to the 1P frequency $\tau \simeq \tau_{1\mathrm{P}}$ show a peak in the kurtosis for the inboard sections, which are more prone to dynamics of the wind velocity component. An explanation is the following: When calculating the increments of an ideal sinusoidal time series using a time lag τ corresponding exactly to the period $\frac{2\pi}{b}$ of a sine wave $f(x) = a \cdot \sin(bx - c) + d$, all increments will be zero. In case the sine is superimposed by other dynamics, say Gaussian white noise, the increments will exhibit Gaussian behaviour and correspondingly a kurtosis of three if the time lag τ is approximately equal to the sine's period so that $\tau \simeq \frac{b}{2\pi}$.

Continuing the discussion of Fig. 8, very small time scales $\tau \leq 1$ sec seem to be dominated by the intermittent wind behaviour. This sensitivity is decreasing towards the blade tip, as the inflow velocity will become more dependent on the rotational velocity component.

It should be mentioned that the summation of the time series of all normal forces for all blades was compared to the thrust time series (cf. Eq. 6). In terms of the kurtosis of increment time series, the model required numerous simplifications in order to arrive at the same result for the thrust and the sum of normal forces, such as: zero cone angle, zero tilt angle, suppression of all DoF for flexible structure, no dynamic stall and more. Finally the time series could be reproduced exactly, also in terms of two-point statistics. This example vividly shows the complexity of a baseline wind turbine model and the number of effects to be taken into account when conducting a similar analysis.

Further on the dynamics of each blade will be summed with those of other blades in the calculation of the rotor thrust or similar other quantities. Dynamics corresponding to deterministic events of a 1P frequency (such as tower-passage or shear), will enter the thrust calculation with a 120 deg phase-shift. This phase-shifted summation will influence the increments statistics and dynamics significantly, in case the period effect is strong enough compared to the contribution of stochastic sources.

The analysis of `RootOOP` led to the analysis of sectional forces for one blade. Still the question remains, why the wind dynamics as shown in Fig. 2, exhibit a much higher kurtosis than the normal forces at the outboard blade sections (cf. Fig. 8). It is well known that the wind velocity component is exceeded in magnitude by the rotational velocity component,

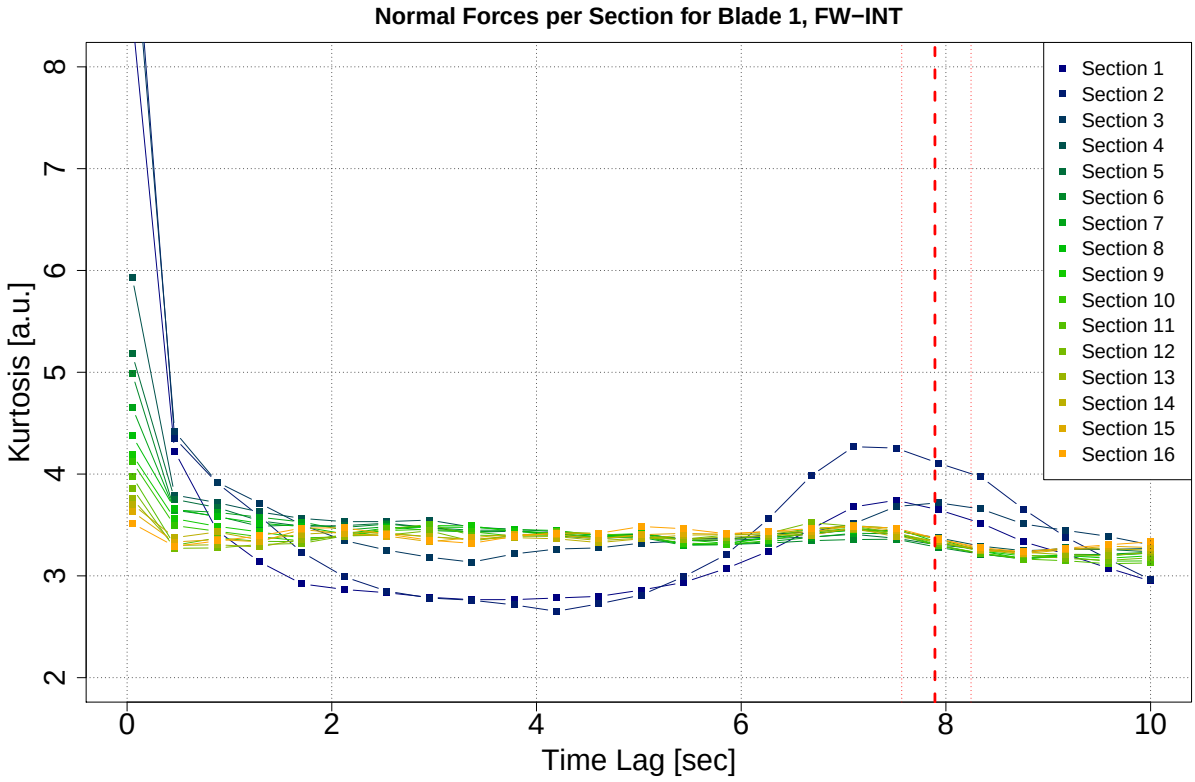

Figure 8: Kurtosis of the probability density of increment time series for the normal forces at each radial section. Section 1 corresponds to the blade root; Section 16 corresponds to the blade tip. The underlying data set is the intermittent case provided by partner ForWind. *Red dashed line:* Period corresponding to the average 1P-frequency ± one standard deviation.

except for at the very inboard sections. Fig. 9 shows the increment kurtosis for the rotor speed ω, which represents the dynamics of the rotational velocity component for all rotor sections as the radius r is constant

$$u_{\mathrm{rot},i} = r_i \cdot \omega \propto \omega. \tag{9}$$

As expected, a high agreement between the dynamics of the outboard section (cf. Fig. 8) and the dynamics of the rotor speed (cf. Fig. 9) is found. It should be emphasized that the intermittent wind fields induce the intermittent dynamics onto the rotational velocity component. This is a key finding, as blade loads are driven by the rotational velocity. Considering previous research work, rotor torque increments were found to exhibit non-Gaussian behaviour (see e.g. Mücke et al. [7]), wherefore it is not surprising that the rotor speed behaves similarly, as these quantities are coupled with each other. Shedding light into the transfer process between the wind field dynamics and the rotor speed dynamics will be a challenge for future research.

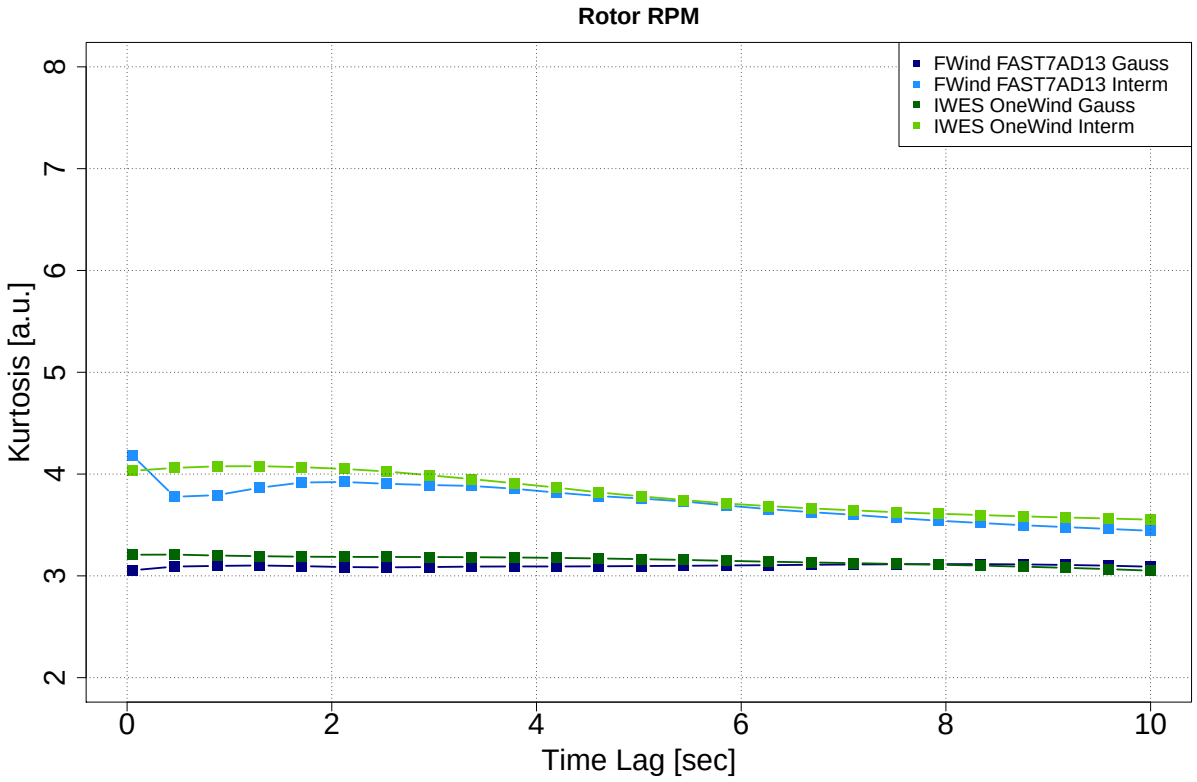

Figure 9: Kurtosis of the probability density of increment time series for the rotor speed time series for all codes and types of fields.

TwBaseFA

Lastly, the dynamics of `TwBaseFA` are discussed. The corresponding kurtosis is displayed in Fig 10. A simple estimation of the tower base bending moment M (in fore-aft direction) is given by the product of hub height h and rotor thrust T, wherefore, intuitively a good agreement between the dynamics of `RotThrust` and `TwBaseFA` is expected.

$$M = h \cdot T \propto T. \tag{10}$$

Fig. 11 shows the direct comparison of both sensors. Especially in the results provided by IWES, the agreement between both quantities is very high. The results provided by ForWind show some deviation. This issue requires further investigation and could not be solved within the time frame of this deliverable. It is likely to arise from some phenomena complicating the relation between thrust and bending moment as outlined in Eq. 10.

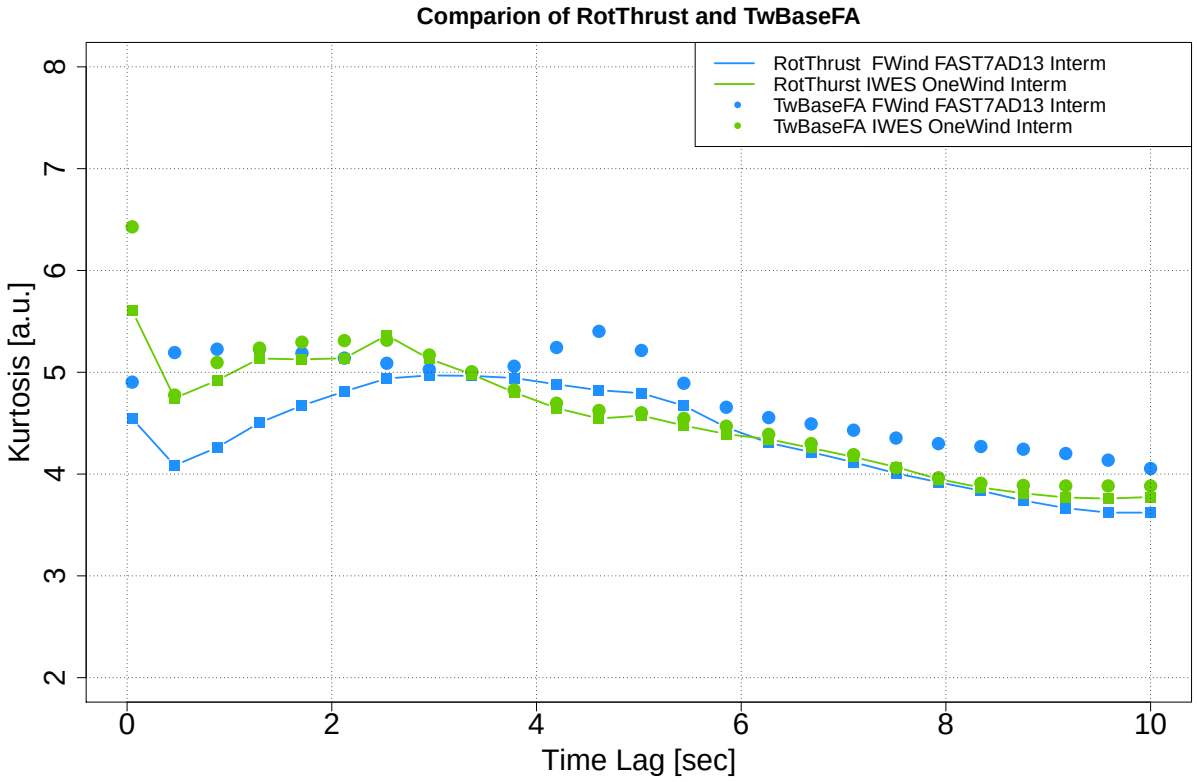

Figure 10: Comparison of the kurtoses of probability density of increment time series for sensors `RotThrust` and `TwBaseFA` for all codes, but intermittent fields only.

Summary

Loads related to one blade (e.g. blade root bending moments) exhibit significantly weaker super-Gaussian statistics as compared to those of the wind fields and correspond to the dynamics of the rotor speed. Again, it shall be emphasized that the rotor speed itself shows super-Gaussian behaviour. Load sensors related to the entire rotor (e.g. rotor thrust, tower base bending and drive train loads) display a strong non-Gaussian behaviour. The latter is not only due to the excitation by the wind field, but can also arise from the phase-shifted superposition of the respective periodic blade dynamics by a shift of 120 deg.

3.3 Damage Equivalent Loads

In this section damage equivalent loads (DEL) related to the IEC 61400 standard [11] are presented. It remains an open question how well the analysis in terms of rain-flow-counting (RFC) satisfies the context of intermittency, as RFC does not consider two-point statistics. It is likely that intermittent two-point statistics will also affect the one-point statistics, wherefore an effect on the DEL may appear; but a more comprehensive investigation regarding

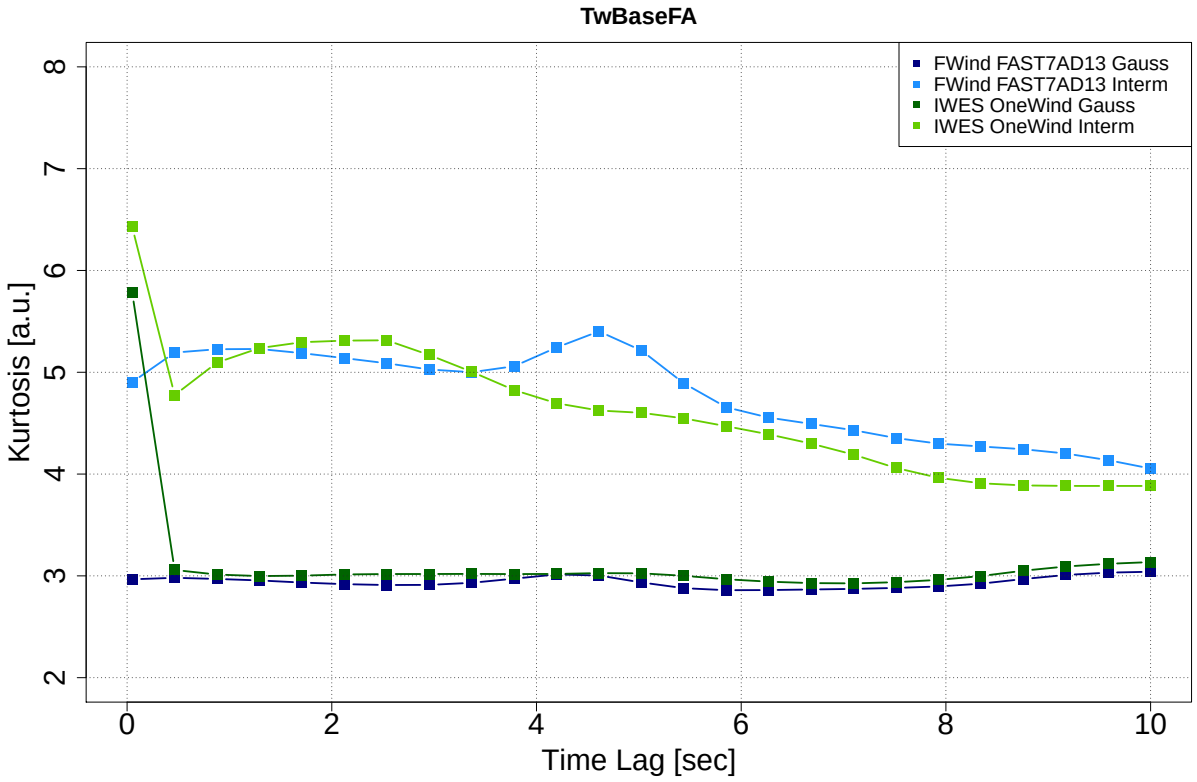

Figure 11: Kurtosis of the probability density of increment time series for sensor `TwBaseFA` for all codes and types of fields.

the suitability of the methodology at hand should be conducted in future work.

Additionally to the Gaussian and intermittent cases, a scaled data set is produced. The scaled data set will have intermittent behaviour, but exactly the same 1st and 2nd statistical moments as the Gaussian one. The scaling procedure can straightforwardly be conducted based on the mean values $\langle x \rangle$ and standard deviations $\sigma(x)$ of the respective time series:

$$x_{\text{scaled}} = \langle x_{\text{Gau}} \rangle + \sigma(x_{\text{Gau}}) \cdot \frac{x_{\text{Int}} - \langle x_{\text{Int}} \rangle}{\sigma(x_{\text{Int}})} \tag{11}$$

In the following, the results of the DEL calculations will be represented in a normalized way as in previous sections. The Gaussian data set provided by partner ForWind was arbitrarily chosen as reference value. The Wöhler exponents were choosen as $m_{\text{Tower}} = 4$ and $m_{\text{Blade}} = 12$ for the tower and blade components, respectively. The reference cycle number was chosen as $N_{\text{ref}} = 10^7$. The results presented in the Figures 12, 13, 14 and in Table 5 do not exhibit a clear trend within the predictions from both codes. While the results provided by partner ForWind show an increase of the DEL for the intermittent cases in the range of

	RootIP	RootOOP	TwBaseFA
FWindFAST7AD13Gauss	100.00	100.00	100.00
FWindFAST7AD13Interm	100.12	107.80	105.18
FWindFAST7AD13Scaled	100.14	111.98	112.58
IWESOneWindGauss	98.38	110.44	71.11
IWESOneWindInterm	98.32	109.44	69.73
IWESOneWindScaled	98.35	114.58	75.51

Table 5: Damage equivalent loads for blade and tower components for all codes and wind fields. Scaling of the intermittent data set according to Eq. 11.

5% – 8% for RootOOP and TwBaseFA, the results provided by partner IWES show a different behaviour: The Gaussian and intermittent case do not differ strongly (within 2%) and even exhibit lower DEL for the intermittent load cases. The sensor RootIP was not expected to exhibit any huge deviations and can be taken as a reference in order to point out potential inconsistencies.

A direct comparison between the scaled results (cf. Eq. 11) and the Gaussian case can not be considered fair, since the former do not arise from the same wind fields (in case of the scaled results the wind field is unknown). Still, scaling emphasizes the importance of load analysis beyond the first two statistical moments.

In future studies, the involved codes must be examined in greater detail regarding modelling differences and maybe even contraries. Also, the work presented in this report should be carried for a larger set of wind fields of the same parametrisation. The wind field generation is a stochastic process, therefore it's properties are likely not sufficiently converged, given the considered amount of data. Since several essential issues and problems needed to be addressed within this study, an extension to a larger number of wind fields was not possible within the available time frame. As mentioned previously, other wind speeds have to be investigated in an analogous manner as well, in order to obtain a comprehensive overview over the impact of intermittency on DEL.

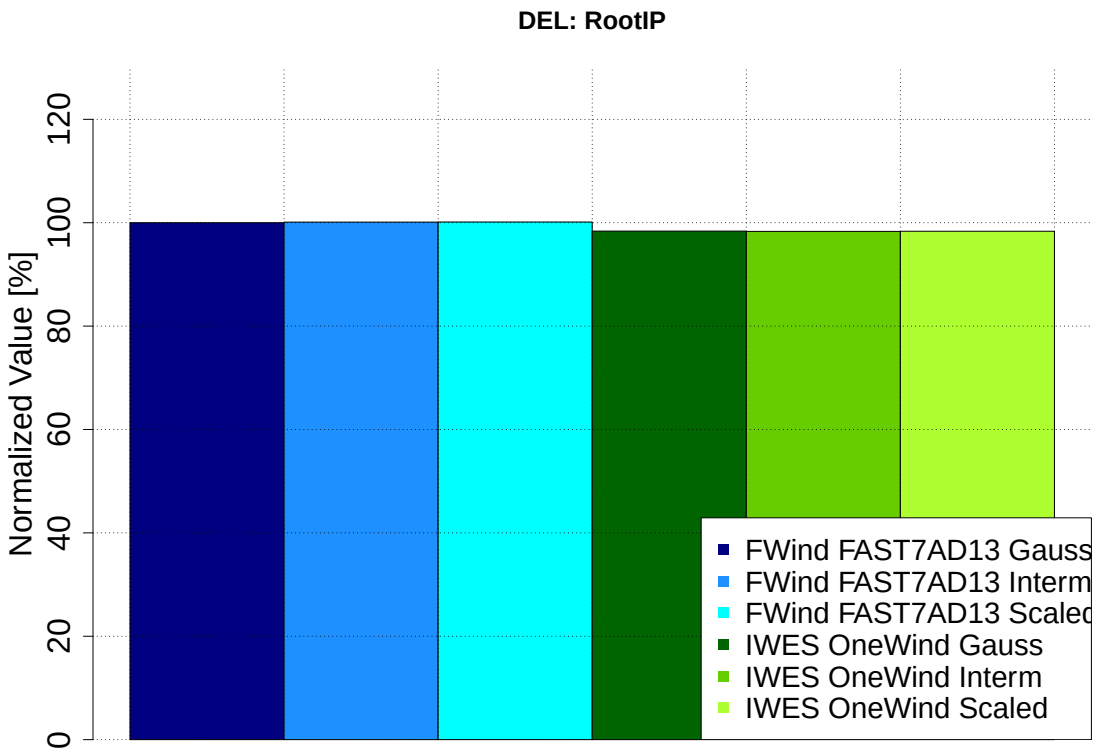

Figure 12: Damage equivalent loads for sensor `RootIP` for all codes and fields. Scaling of the intermittent data set according to Eq. 11.

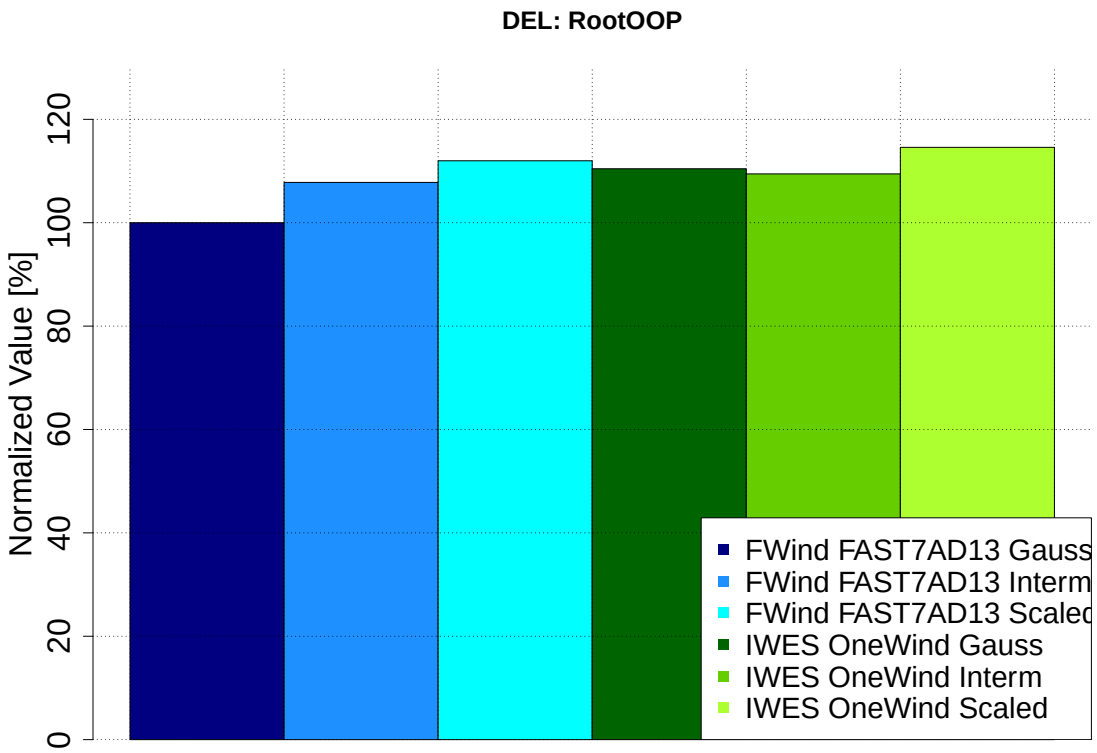

Figure 13: Damage equivalent loads for sensor `RootOOP` for all codes and fields. Scaling of the intermittent data set according to Eq. 11.

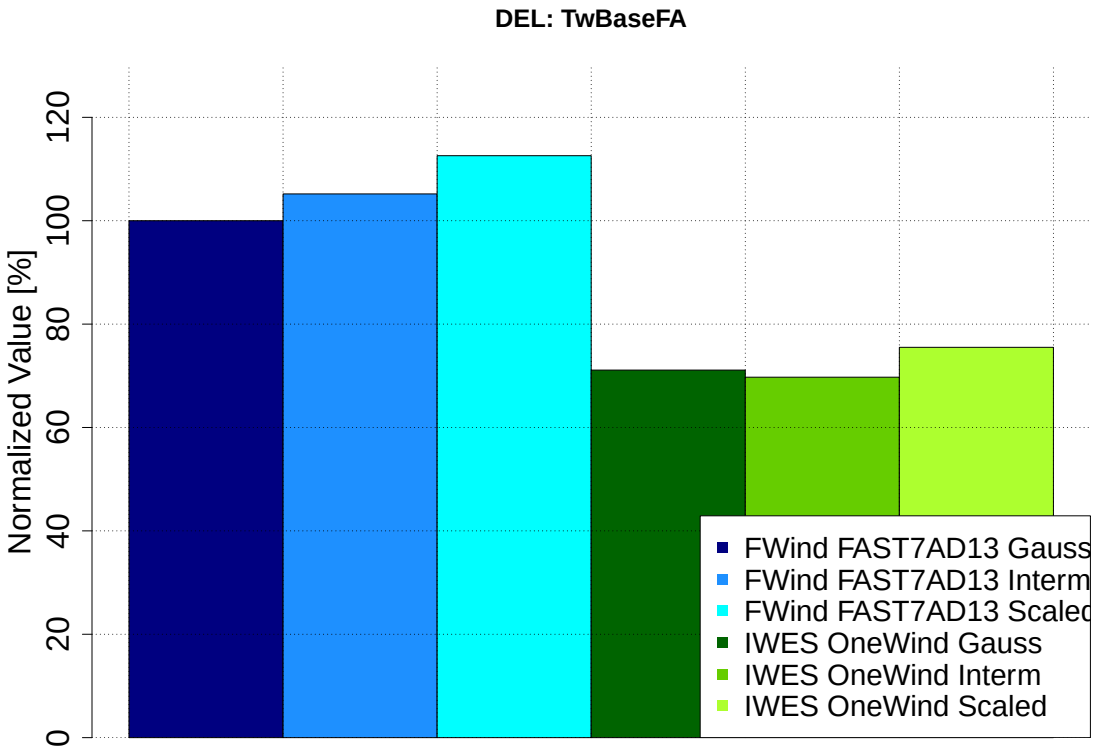

Figure 14: Damage equivalent loads for sensor `TwBaseFA` for all codes and fields. Scaling of the intermittent data set according to Eq. 11.

4 Summary and Conclusion

In this section, the findings of this study will be summarized.

Comparability of codes

In the presented study different aero-elastic codes were compared with respect to the question how they process intermittent fields. Overall, a good agreement between the codes regarding two-point statistics was found (see Sec. 3.2), given that different codes and underlying modelling approaches were used. Differences in the one-point statistics were discovered, which are very likely arise due to modelling differences (see Sec. 3.1). Future work should follow the concept of this investigation and aim to minimize differences in the modelling in order to obtain a clearer picture.

Damping of intermittent dynamics

A clear trend, indicating a damping of intermittent dynamics, more precisely the standard deviation for all relevant sensors, was observed (see Sec. 3.1). A possible explanation was brought forward in the corresponding discussion. It is important to record that this damping must not be understood as a removal of the dynamics of interest from the time series, as became evident in futher discussions (see Sec. 3.2).

Numerical intermittency

The emergence of numerical intermittency was observed and discussed (see Sec. 3.2). Future work should include an examination with respect to numerical intermittency for all involved codes, as this effect has the potential to distort the results obtained in comparable studies. It can arise from relaxation and time delay filters within aero-elastic codes, which are often used in order to stabilize computations. This issue does not arise from physical modelling, but from numerics and software development.

Transfer function between wind and rotor thrust

Another aspect of this study aims at gaining a better understanding how the dynamics in the wind field are processed between different wind turbine components. Straightforwardly, basic relations between the dynamics of different quantities can be derived, as for example in Eq. 8. Actually, these basic relations are often complicated by a number of effects, which act as non-linear filters and modify the dynamics. Two-point statistics are highly sensitive to effects, that are usually not paid too much attention to. One example is numerical intermittency as discussed previously. Other well understood concepts such as rotor cone, blade-tower passage and motion due to structural flexibility can modify the dynamics in complex fashion. Therefore a prediction and sometimes even the sheer understanding of the

two-point behaviour is very challenging, as periodic signals (e.g. due to the rotor rotation) interact with stochastic processes (e.g. due to wind dynamics) in a highly non-linear manner.

Non-Gaussian behaviour of $u_{\mathbf{rot}}$

In the context of loads, the rotational velocity component u_{rot} or simply the rotor speed ω is of high interest, as it will drive blade loads. It was found that ω exhibits super-Gaussian behaviour, which in return will lead to super-Gaussian behaved blade load increments. As discussed previously, the formulation of a transfer function between different quantities is very challenging. Anyhow, bringing understanding how the rotor speed ω is excited by the wind dynamics is highly interesting and involves all possible system dynamics.

Fatigue load anlysis

In order to judge the relevance of turbulence intermittency with respect to wind turbine loads, Damage Equivalent Loads (DEL) were compared (see Sec. 3.3). No clear trend could be found between both codes utilized in this study. One data set indicated a sensitivity to intermittency in the DEL in the range of 8% (for the wind speed of 9 $\frac{m}{s}$). The other data set showed less sensitive in the range of 2%. More data must be considered in this context in order to arrive at final conclusion. Anyhow, intermittency seems to be potent to influence DEL.

5 Open issues and future work

Open questions and weaknesses of the presented investigation are addressed in this section, in order to provide guidance for future research projects.

Wind shear

The wind fields considered in this study did not feature a wind shear. It is well known that wind shear will induce strong periodic dynamics corresponding to the 1P frequency onto several quantities. Therefore it is expected to impact the two-point statistics of the entire system significantly. Wind shear was excluded from this study for the sake of simplicity, but should be considered in future work.

Other wind velocities

In order to estimate the impact of intermittency, the current study needs to be conducted for a large range of wind speeds. This is obviously related to the complication of several dynamics, for example when entering the pitch regulated wind speed regime. Since several essential problems needed to be addressed in this study, the consideration of further wind speeds was not possible within the scope of this deliverable.

Spectral properties of wind fields

A weak spot of the used wind field generator lies in the spectral properties of the generated fields. Future work towards the generation of wind fields with common wind spectra according to Mann [12] or Kaimal et al. [13] using the Continuous-Time-Random-Walk (CTRW) model should be undertaken.

Continuation of code comparison

As mentioned above, deliverable D4.7 was meant to be carried out by ForWind solely. A highly valuable contribution was made by partner IWES in form of reference computations. Future work should focus on a more strict comparison of the used codes. Comparable models with similar performances are required in order to arrive at consistent conclusion with respect to the impact of turbulence intermittency. The study conducted within D4.7 provides a helpful outline and can be used as a basis for future work.

Amount of data

Overall, more data is required in order to make the conclusion drawn from this work more reliable. More aero-elastic codes should be considered in a future study, as well as a wide

range of wind speeds and even other wind turbines. First and foremost, a larger sample of wind fields needs to be considered in order to assure the findings are statistically significant.

References

[1] F. Böttcher, C. Renner, H.P. Waldl, and J. Peinke. On the statistics of wind gusts. *Boundary Layer Metereology*, 2003.

[2] J. M. Vindel, C. Yagüe, and J. M. Redondo. Structure function analysis and intermittency in the atmospheric boundary layer. *Nonlinear Processes in Geophysics*, 2008.

[3] A. Morales, M. Wächter, and J. Peinke. Characterization of wind turbulence by higher-order statistics. *Wind Energy*, 2012.

[4] Website of the research platforms in the North Sea and Baltic Sea (germ. abr. FINO). `http://www.fino-offshore.de/de/`, as of August 2016.

[5] M. Wächter et al. Wind energy and the turbulent nature of the atmospheric boundary layer. *Journal of Turbulence*, 2012.

[6] P. Milan, M. Wäechter, and J. Peinke. Turbulent character of wind energy. *Physical Review Letters*, 2013.

[7] T. Mücke, D. Kleinhans, and J. Peinke. Atmospheric turbulence and its influence on the alternating loads on wind turbines. 2011.

[8] D. Kleinhans. *Stochastische Modellierung komplexer Systeme.* PhD thesis, 2008.

[9] H. Gontier, A. P. Schaffarczyk, D. Kleinhans, and R. Friedrich. A comparison of fatigue loads of wind turbine resulting from a non-gaussian turbulence model vs. standard ones. *Journal of Physics: Conference Series*, 2007.

[10] J. Berg, A. Natarajan, J. Mann, and G. Patton. Gaussian vs non-gaussian turbulence: impact on wind turbine loads. *Wind Energy*, 2016.

[11] International Electrotechnical Commision. International standard 61400: Wind turbines. Technical report, 2005.

[12] J. Mann. The spatial structure of neutral atmospheric surface-layer turbulence. *Journal of Fluid Mechanics*, pages 141–168, 1994.

[13] J. C. Kaimal, J. C. Wyngaard, Y. Izumi, and O. R. Cote. Spectral characteristics of surface-layer turbulence. *Q.J.R. Meteorol. Soc.*, pages 563–598, 1972.

[14] Garrad Hassan & Partners Ltd. Bladed theory manual version 4.0. Technical report, 2010.

[15] J. M. Jonkman and M. L. Buhl. FAST User's Guide. Technical Report EL-500-38230, National Renewable Energy Laboratory, Colorado, August 2005.

[16] P. J. Moriarty and A. C. Hansen. AeroDyn Theory Manual. Technical Report NREL/TP-500-36881, National Renewable Energy Laboratory, 2005.

[17] R. Pereira, G. Schepers, and M. Pavel. Validation of the BeddoesLeishman dynamic stall model for horizontal axis wind turbines using MEXICO data. 2012.

[18] Website of the International Wind Agency (IEA). `https://www.ieawind.org/taskWebSites.html`, as of August 2016.

[19] Garrad Hassan & Partners Ltd. Bladed user manual. Technical report, 2010.

[20] M. Strobel, F. Vorpahl, C. Hillmann, X. Gu, A. Zuga, and U. Wihlfahrt. The OneWind Modelica Library for Offshore Wind Turbines - Implementation and first results. Technical report, Fraunhofer Fraunhofer Institute for Wind Energy and Energy System Technology, Bremerhaven.

[21] P. Thomas, X. Gu, R. Samlaus, C. Hillmann, and U. Wihlfahrt. The OneWind Modelica Library for Wind Turbine Simulation with flexible Structure - Modal Reduction Method in Modelica. Technical report, Fraunhofer Fraunhofer Institute for Wind Energy and Energy System Technology, Bremerhaven, 2004.

[22] B. J. Jonkman and K. Kilcher. TurbSim User's Guide: Version 1.06.00. Technical report, National Renewable Energy Laboratory, Colorado, 2012.

[23] J. Jonkmann, S. Butterfield, W. Musial, and G. Scott. Definition of a 5-MW Reference Wind Turbine for Offshore System Development. Technical Report TP-500-38060, National Renewable Energy Laboratory, Colorado, February 2009.

Overview: OneWind Modelica Library

Environment	Wind	• Exponential Wind Shear • Constant wind • Deterministic Wind • Turbulent Wind (Kaimal) • Gust models
	Waves	• Linear waves (Airy theory) • Linear irregular waves based on Pierson-Moskowitz and JONSWAP spectrum • Stretching Methods (Wheeler- and Delta stretching)
	Ice	• Floating ice loads
	Soil	• Linear spring-damper • *p-y-approach*[1]
Aerodynamics		• Blade element momentum theory (BEM), dynamic stall Beddoes and Oye • General dynamic wake (GDW), dynamic stall Beddoes and Oye • Eddy viscosity wake
Hydrodynamics		• Morisons equation
Structural Models	Rotor Blade	• rigid model • finite element model based on Euler-Bernoulli beam theory • modal reduced model as presented in [21]

	Hub and Nacelle	• Rigid Nacelle
		  • rigid drivetrain
		  • fixed speed generator model
		• Flexible nacelle
		  • flexible drivetrain (torsional DOF)
		  • variable speed generator model

	Tower	• rigid model • finite element model based on Euler-Bernoulli beam theory • modal reduced model as presented in [21]

	Substructure	• Monopile
		  • rigid model
		  • finite element model based on

		Euler-Bernoulli beam theory • modal reduced model as presented in [21] • *Jacket*[1] • *Tripod*[1] • *Spar Boye*[1] • *Semisubmersible*[1]
Operating control		• Discrete and continuous (NREL 5-MW [23]) • including of dynamic link library (dll) possible • Pitch and torque control • Yaw control

Table 6: Overview on the environmental and structural models of the OneWind Modelica Library

[1] under development